Research article

Sub-pixel Mineral Mapping of Serpentine and Magnesite for Chromite Exploration, Using Hyperion (EO1) Images

Saeed Khojastehfar[1]*, Hojatollah Ranjbar[1], Shahram Shafiei Bafti[2]

1- Dept. of Mining Engineering, Shahid Bahonar University of Kerman, Kerman, Iran
2- Dept. of Geology, Shahid Bahonar University of Kerman, Kerman, Iran

*Corresponding author: E-mail: *e.saeedkhojastehfar@gmail.com*

Keywords	Abstract
Remote sensing **Hyperion** **Chromite** **Alteration** **Serpentine** **Magnesium**	Abdasht chromite mine is located in the ultramafic complex of southern Iran, which has abundant chromite reserves such as Soghan, Esfandagheh, Faryab, etc. The main purpose of this study was to investigate the capability of Hyperion in the alteration mapping related to chromite mineralization in the Abdasht area, south of Kerman Provine, Iran. Since serpentine and magnesite have been observed associated with chromite in this area, mapping of these minerals can be used for the exploration of chromite. For this purpose, atmospheric correction/calibration was performed on the

Hyperion images. The representative samples collected from the outcrops in the area were tested in the laboratory of the Iranian Space Agency and the spectra of serpentine and magnesite were extracted. Serpentine and magnesite were mapped, using Spectral Angle Mapper (SAM) and Matched Filtering (MF) methods. In order to verify and control the results, a field visit has been made to the area. The obtained classification accuracy for serpentine obtained from MF and SAM methods were 87% and 81%, respectively. Magnesite map showed an overall accuracy of 65% and 60% for MF and SAM methods, respectively. The lower accuracy of magnesite can be attributed to its small extent in the field. It is suggested that due to the power of Hyperion images in the detection of chromite-bearing serpentine rocks, these images can be used for the exploration of chromite.

1. INTRODUCTION

The study area is located in the south of Kerman Province in Iran and 50 km east of Orzueeyeh City with latitudes of 56°43'00" to 56°48'00" north and longitudes 28°20'00" to 28°24'00" east (Figure 1). This area is part of the mafic-ultramafic rock belt of central Iran. In this area, there are many units of mafic and ultramafic rocks, the most important of which include the Sikhoran, Soghan, and Abdasht complexes. These complexes are part of the Esfahadeh ophiolite complex, which are located in the Sanandaj-Sirjan

zone and are considered areas rich for Iranian chromite mineralization. Chromite exploration methods are diverse and include geochemistry, geophysics, remote sensing, and geology. Researches have been done in the field of chromite exploration using satellite images, in recent years [1, 2, 3, 4, 5]. Researchers have worked on hyperspectral images and different types of alteration were identified [6, 7, 8, 9, 10, 11]. They have studied ophiolites and associated alterations with the use of satellite imageries for the exploration of chromite deposits. According to NASA's New Millennium Plan, the Earth Observer

Satellite (EO1) was launched on November 21, 2000. Hyperion is a hyperspectral sensor installed on this satellite and is able to cover 0.5-2.5 micrometers spectral range with a spectral resolution of 10 nm and a spatial resolution of 30 meters. This sensor has an imaging width of 7.65 km and a length of 185 km. The altitude of this sensor is 705 km above the ground and it captures images in 242 spectral bands, of which bands 1-70 are in the visible and near-infrared range and bands 71-224 are located in the short infrared range [12, 13]. The focus of this study is to investigate the ability of Hyperion images to map minerals due to the secondary alteration of ultramafic massifs in the southern part of the Abdasht chromite mine. Spectral Angles Mapper (SAM) and Matched Filter (MF) are used in conjunction with field studies and laboratory analyses.
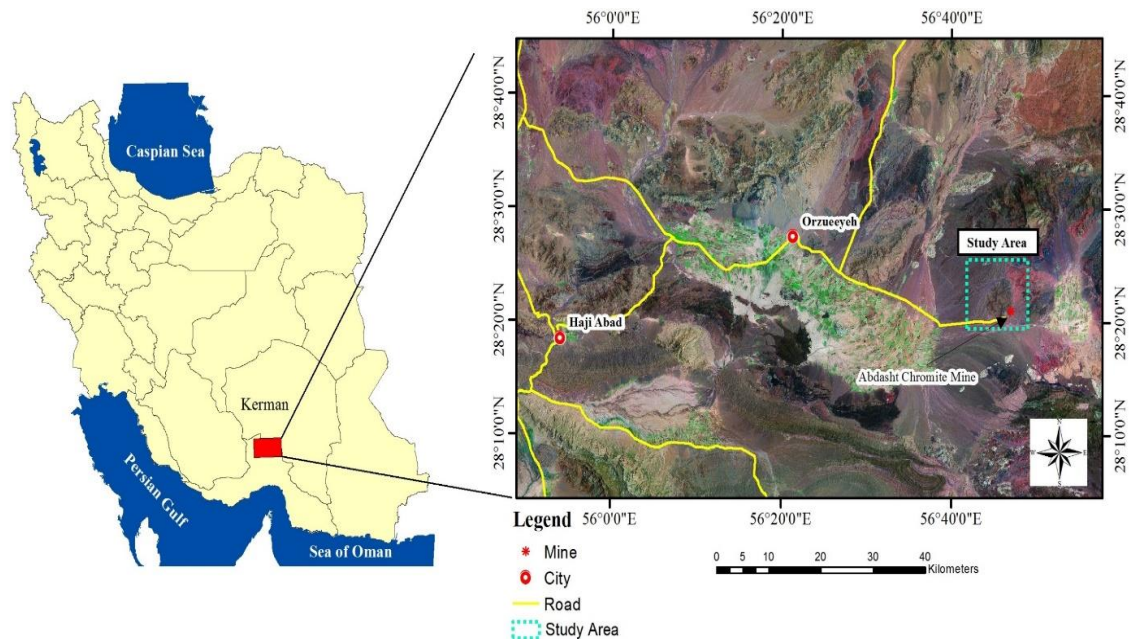
Fig.1. Geographical location and access routes of the study area.

2. GEOLOGY AND MINERALIZATION

The Abdasht ultramafic massif is part of the Esfahadeh ophiolite assemblage, located in the Sanandaj-Sirjan structural zone [14] and also in the Paleozoic metamorphic complex [15]. Abdasht ophiolitic massif consists of relatively high hills and mountains with a length of 8 km and a width of about 5 km. This mass is composed of ultramafic rocks with more or less regular periodicity of peridotites, including dunite and harzburgite, which are converted to dunite-wehrlite and dunite-lherzolite. Peridotites in this area are often serpentinized. Alteration and surface decomposition are also seen in these peridotite rocks (Figure 2). Crystalline magnesite mineral is abundant in Abdasht massif, so that rock fractures are filled with magnesite. These magnesite veins have economic value and can be considered in some areas due to their good purity and also the large size of the veins. Magnesites are the result of the alteration and dissolution of dunite, serpentinite rocks and their deposition along the fractures and the faults. The potential reserve of the Abdasht mine is 8 million tons of chromite (Cr_2O_3) with a grade of 41% [16].
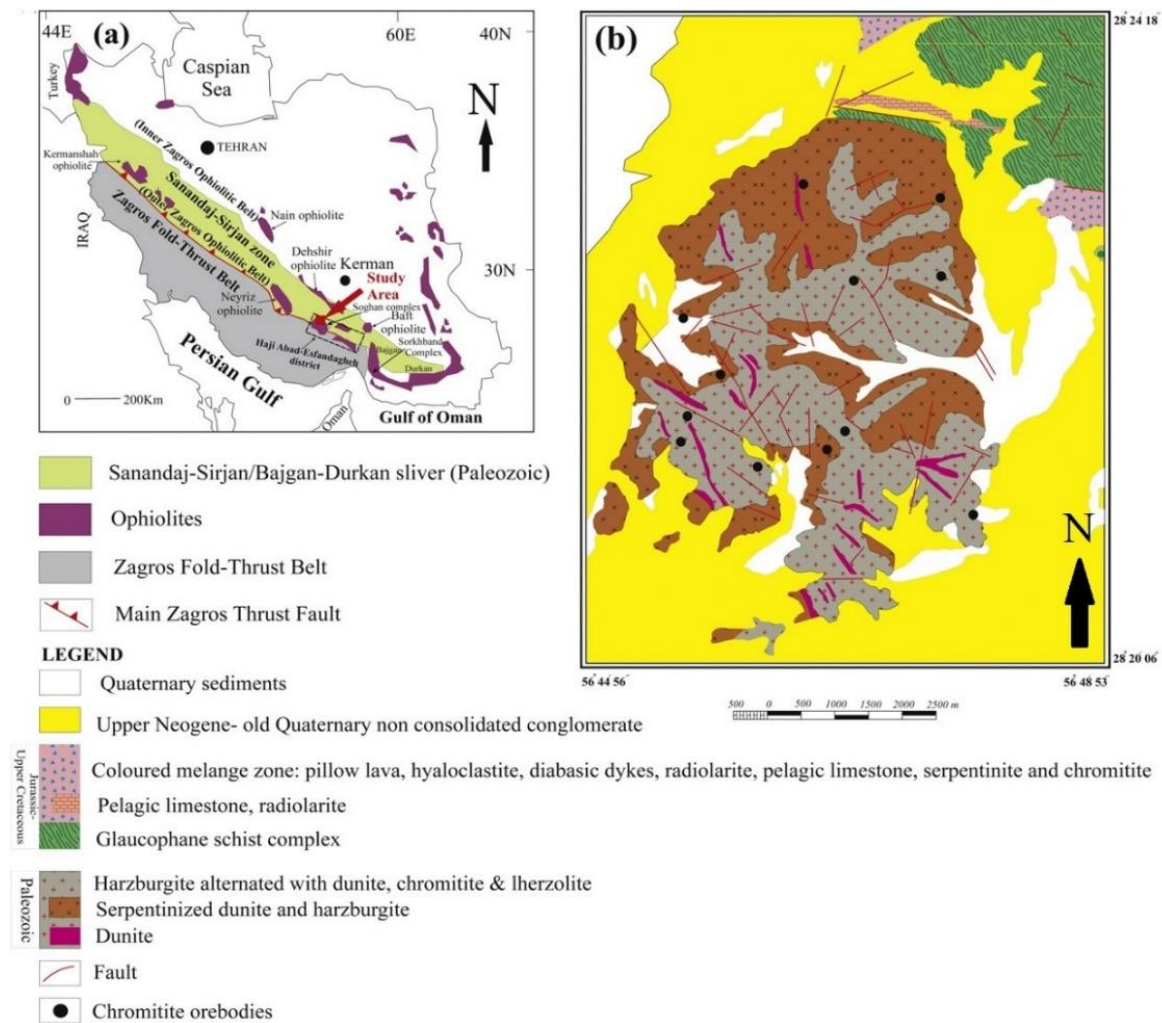
Fig.2. A: The location of the study area is within the ophiolite belts of Iran and the south of the Sanandaj Sirjan zone. B: Simple geological map of Abdasht complex (Najafzadeh and Ahmadipour, 2016).

3. DATA AND METHODS

The Hyperion sensor data used in this study is at Level_1R (L1R), which has the lowest level of preprocessing. Level_1T images have not been corrected for image geometry and radiometric/atmospheric corrections. In this study, Hyperion images were used with scene number EO1H1600402015303110KF_1R and with path and row of 60 and 40 respectively, which were acquired on 30/10/2015.

In order to obtain information about the spectral properties of alteration minerals in the area, a number of field samples were collected. Spectral measurements on these samples were done using the FieldSpec device in Iran Space Laboratory. Then, the extracted spectra were used for mapping magnesite and serpentinite using SAM and MF methods. Finally, in order to evaluate the overall accuracy of the results, a field visit was conducted to the study area and the classification accuracy of both methods was determined.

3.1. Preprocessing Data

Hyperion images include many errors such as: defective bands, embedded lines, banding effect, and spectral smile, which must be corrected before proceeding further for image processing the images. In general, the following algorithm is recommended for the pre-processing of Hyperion images (Figure 3).

```
┌──────────────┐     ┌──────────────┐     ┌──────────────┐     ┌──────────────┐
│ Removing the │ ──▶ │Correcting for│ ──▶ │  Converting  │ ──▶ │    Smile     │
│   defective  │     │ the missing  │     │   DN to      │     │  correction  │
│    bands     │     │     line     │     │  radiance    │     │              │
└──────────────┘     └──────────────┘     └──────────────┘     └──────────────┘
                                                                        │
                                                                        ▼
┌──────────────┐     ┌──────────────┐     ┌──────────────┐
│Noise removal │     │Correcting the│     │ Atmospheric  │
│by using MNF  │ ◀── │ destripping  │ ◀── │ correctin by │
│and softening │     │              │     │              │
│of spectra    │     │              │     │              │
└──────────────┘     └──────────────┘     └──────────────┘
```
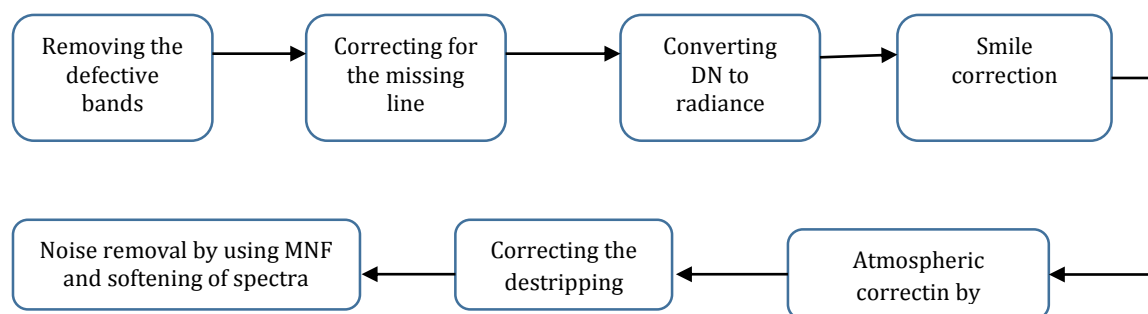
Fig. 3. Hyperion image correction method.

The first step in pre-processing of Hyperion images is to remove the defective bands that occur due to the poor performance of its detectors, and the pixel values are recorded as zero, which results in dark pixels in Hyperion images. Therefore, bands with zero values and high-noise images were identified and deleted [12], and finally, 155 spectral bands were selected for processing (Table 1). In another study [17, 18] selected 155 spectral bands. Also, the lines embedded in each band were visually eliminated by averaging the two adjacent pixels.

Table 1. Bands used to process Hyperion sensor data in this research

	Bands	Wavelength range (nm)
Visible and near infrared	8-57	426.81 - 925.4
Short wavelength infrared	79	932.63
	83-119	972.99 - 1336.15
	133-164	1477.43 - 1790.18
	183-184	1981.86 - 1991.95
	188-220	2032.35 - 2355.20

To Convert DN to a radiance unit, VNIR and SWIR bands were divided by 40 and 80 respectively. The values of the output pixels are in $W / (m^2 * sr * \mu m)$ and since for FLAASH atmospheric correction input, the images must have a $\mu W / (cm^2 * sr * nm)$ unit, Therefore, these numbers are divided by 400 for VNIR bands and 800 for SWIR bands, in order to convert the pixel values to radiance [12, 19, 20]. The spectral curvature error, known as Smile or Frown, is caused by push-up imaging technology and is present in all Hyperion data [19]. The presence of a spectral smile in the hyperspectral images appears in the first components of the MNF conversion as a gradient, which was corrected by adjusting the mean column in the radiance space on the VNIR range. In this method, for each single band of Hyperion data, the average value of each column is set equal to the average value of the

band. FLAASH correction is used to perform atmospheric correction and the parameters in Table 2 are used for this correction [21]. Vertical stripping error is another error in Hyperion images that was corrected using the Vertical Strip Removal module (Figure 3). Residual noise after atmospheric correction includes two specific types. The first noise is related to the detectors and the amount of low signal-to-noise, which generally have spectral and spatial correlations or local correlations to the detector geometry and spatial correlations related to their shooting scene. Another noise is related to systematic effects that occur due to the difference between the actual model and the atmospheric model selected for the imaging range [20]. This type of noise can be improved by using the Spectral Polishing model [27, 28, 29]. In this method, the curves are the spectral image of soft polynomial functions or splines is fitted and the small difference is interpreted as noise, which by removing them increases the accuracy of the reflectivity. To eliminate residual noise, the first 11 components of MNF for the VNIR images and the first 12 components of MNF for the SWIR images were used and the other components were removed due to higher noise, then the components used were inverted to the original space in order to obtain reduced noise data. Figure 4 shows the spectra extracted from the images before and after the correction.

Table 2. Selected parameters for flash correction based on selected file metadata and models

Image center coordinates	Long: 56.74253889 Lat: 28.30366389
Sensor distance from the ground	705km
The average height of the area above sea level	1500 m
Shooting date	2015/10/30
Shooting time	04:58:38
Atmospheric model	Tropical
Aerosol model	Rural
Pixel size	30m
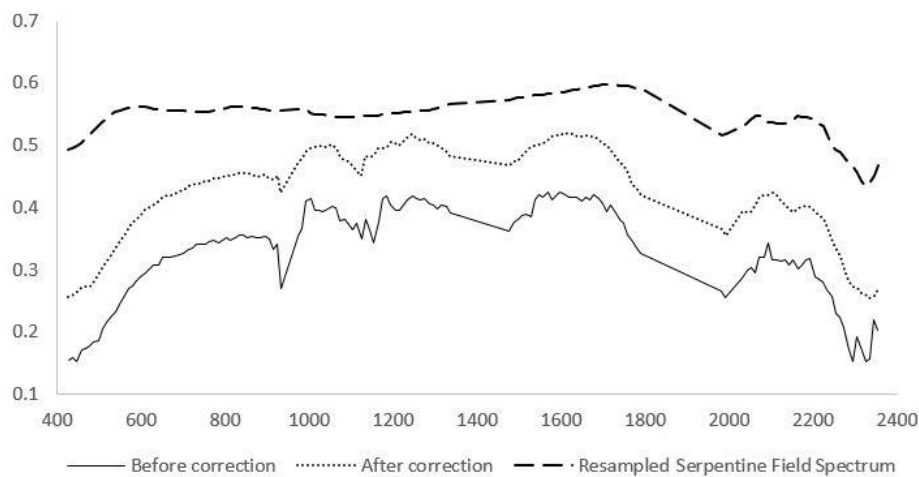
Fig.4. FieldSpec3 serpentine field spectrum with satellite image spectrum before and after corrections.

3.2. Field Spectrum Data Collection Operations ASD﹙Field Spec3®﹚.

In the study area, 24 samples were taken from 8 regions. In each area, three samples with high, medium and low alteration intensities were collected from the Abdasht chromite mine and the spectra were measured in the laboratory of the Iranian Space Agency, using the Fieldspec3 spectroradiometer. Serpentine shows strong adsorption properties at 1.4 and 2.3 μm and a weaker adsorption at 1.95 μm. The above absorption curves are attributed to the presence of water and harmonic vibrations and the combined vibrations involved in the OH states (Figure 5). Magnesite with the chemical formula $MgCO_3$ is formed by the chemical reaction of CO_2 which is present in atmospheric water on serpentine and ultrabasic rocks, which is generally associated with chromite deposits. Magnesite has absorption bands in the 1.87, 1.98, and 2.30 micrometers (Figure 6).

In the study area, 24 samples were taken from 8 regions. In each area, three samples with high, medium, and low alteration intensities were collected from the Abdasht chromite mine and the spectra were measured in the laboratory of the Iranian Space Agency, using the Fieldspec3 spectroradiometer. Serpentine shows strong adsorption properties at 1.4 and 2.3 μm and a weaker adsorption at 1.95 μm. The above absorption curves are attributed to the presence of water and harmonic vibrations and the combined vibrations involved in the OH states (Figure 5). Magnesite with the chemical formula MgCO3 is formed by the chemical reaction of CO2 which is present in atmospheric water on serpentine and ultrabasic rocks, which is generally associated with chromite deposits. Magnesite has absorption bands in the 1.87, 1.98, and 2.30 micrometers (Figure 6).

Fig. 5. Results of spectral measurment of serpentine samples (S-SE1) from Abdasht mine. S: Surface of the sample with low alteration. M: surface of the sample with moderate alteration and H: surface of the sample with high alteration.
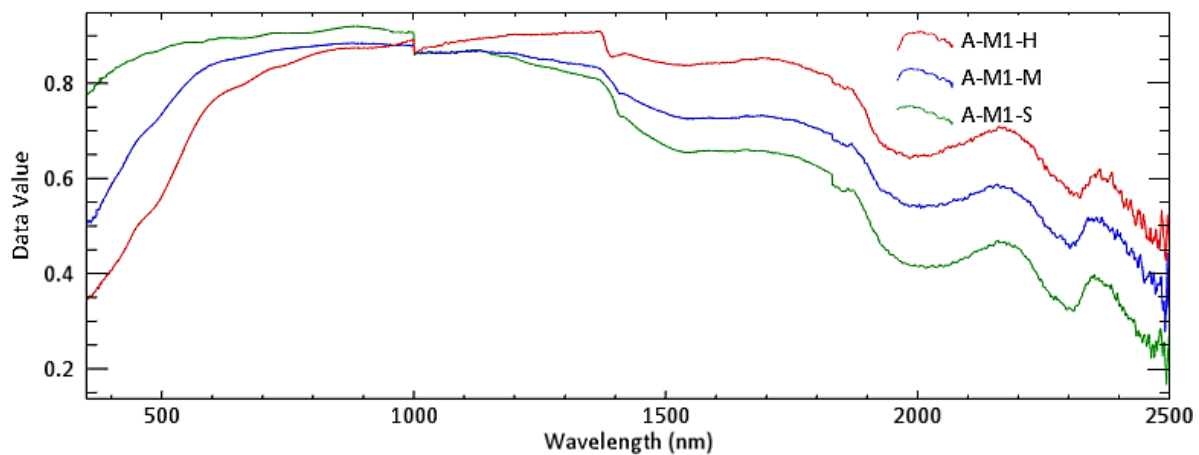
Fig. 6. Results of spectral measurement of magnesite sample (A-M1) from Abdasht mine. S: Spectral analysis on the surface of the sample with low sample alteration. M: Spectral analysis on the surface of the sample with moderate sample alteration. H: Spectral analysis on the surface of the sample with high sample alteration.

3. 3. Mapping Alterations By Spectral Angle (SAM) Method

The SAM method is applied by many researchers in remote sensing studies for mineral exploration [22, 23]. It uses an n-dimensional angle to match pixels to reference spectra. The spectra are converted into vectors. The algorithm determines the spectral similarity between the image and reference spectra by calculating and comparing the cosine value of these two spectra (vectors).   The cosine value can be computed using Equation. 1, where n_b, t_i and r_i are number of bands, reflectance of band i for image spectrum, and reflectance of band i for reference spectrum, respectively as follows:

$$cos\, a = \frac{\sum_{i=1}^{nb} t_i \cdot r_i}{\sum_{i=1}^{nb} t_i^2 \cdot \sum_{i=1}^{nb} r_i^2} \qquad (1)$$

The result of SAM is presented by a rule and classification images. The pixel values in the rule image represent the angle.

3. 4. Mapping Alterations By Matched Filtering (MF) Method

Matched filtering (MF) is used to find the abundances of user-defined end members using a partial unmixing. This technique maximizes the response of the known end member and suppresses the response of the composite unknown background, thus "matching" the known signature. The results of the MF appear as a series of gray-scale images (fraction maps), one for each selected end member. These fraction maps have values that range from 0 to 1, where 0 represents a non-match to the end member (training) spectrum and 1 represents a perfect match [24, 25, 26].

4. RESULTS AND DISCUSSION

Based on the results, several types of alterations have been distinguished using SAM and MF which have been confirmed by field studies. For example, based on the results, some amounts of magnesite can be expected in the northeastern and southeastern areas of the Abdasht chromite mine associated with serpentine alteration, based on field visits in these areas, the presence of magnesite veins in the serpentine bearing areas were confirmed. Also, after detecting serpentine alteration in the region, it was determined that serpentine alteration has been detected in the sediments northwest of Abdasht mine, according to the geological map of the region, these sediments originates from the upstream area of the mine due to the transport of altered serpentinized rocks. Although Hyperion satellite images have high spectral resolution, but the low spatial resolution does not allow the identification of chromite mineralization in the form of lenses and small streaks. This can be improved by image fusion of Hyperion images with high resolution images.
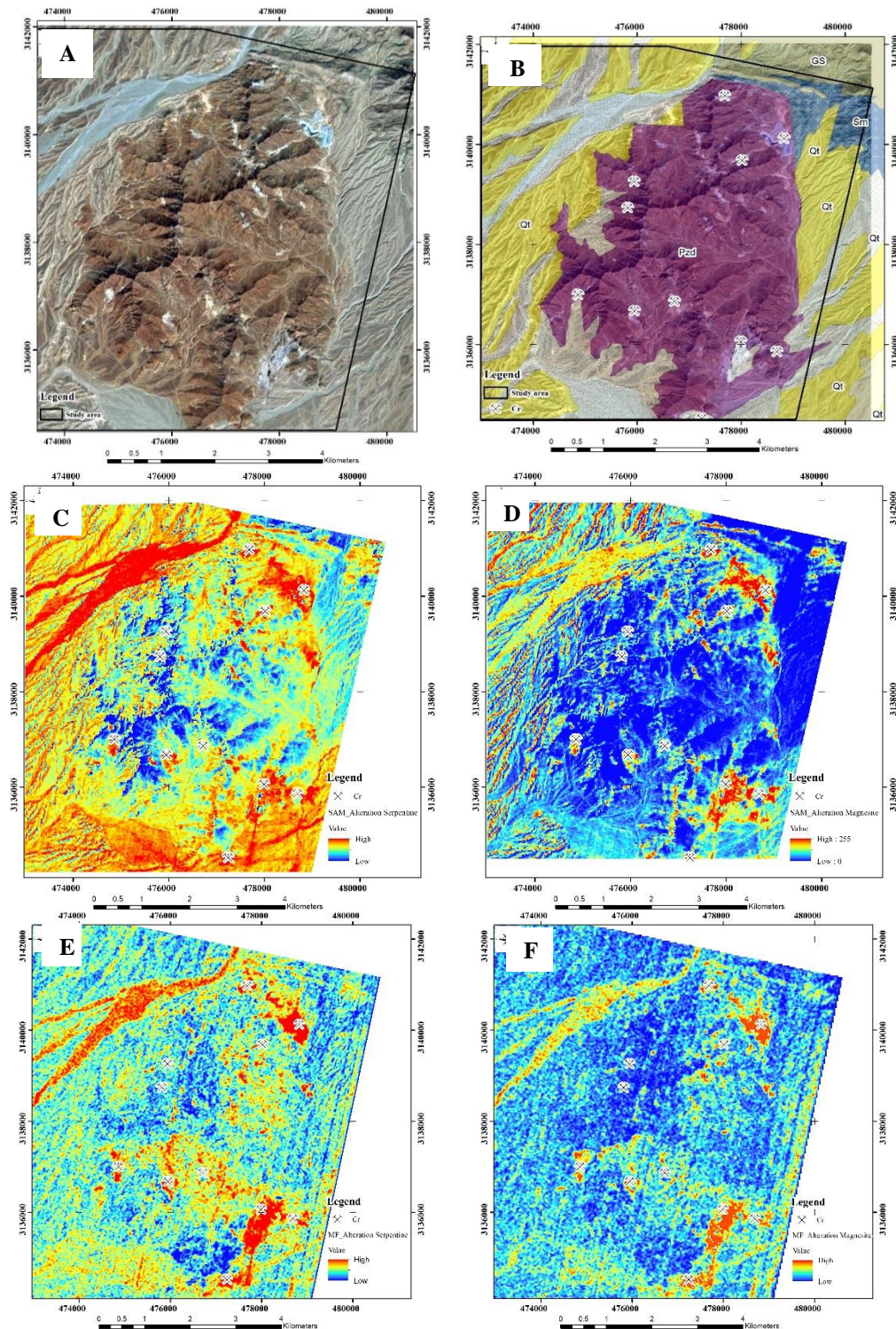
Fig. 7. A) Hyperion Satellite image RGB(29,20,11) of Abdasht massif. B) Geological map of Abdasht chromite mine with index of active mines (Pzd: Dunite, Harzburgite, chromitite, olivine, . Gs: Glaucophane schist. , Sm: Alternation of calcschist, Marbel, epidote-muscovite . Qt: High level,older piedmont alluvial fan). C) Detection of serpentine using spectral angle method. D) Detection of magnesite using SAM method. E) Detection of serpentine alteration using MF method. F) Detection of magnesite alteration using the MF method.

5. ACCURACY ASSESSMENT

The results obtained through this study were evaluated by sampling and field visits performed on serpentine and magnesite outcrops and the overall accuracy method was calculated (Figures 8 and 9). The overall accuracy is calculated by summing the number of pixels classified correctly, divided by the total number of pixels. The classification accuracy of MF and SAM methods for

serpentine alteration are 87% and 81%, respectively, and for magnesite 65% and 60% (Table 3). Probably, the low accuracy of magnesite is due to its small spatial extent in the area. Figure

8 shows the outcrops of serpentine alteration and magnesite in the area. Many of the collected samples from the area are depicted in figure 9.
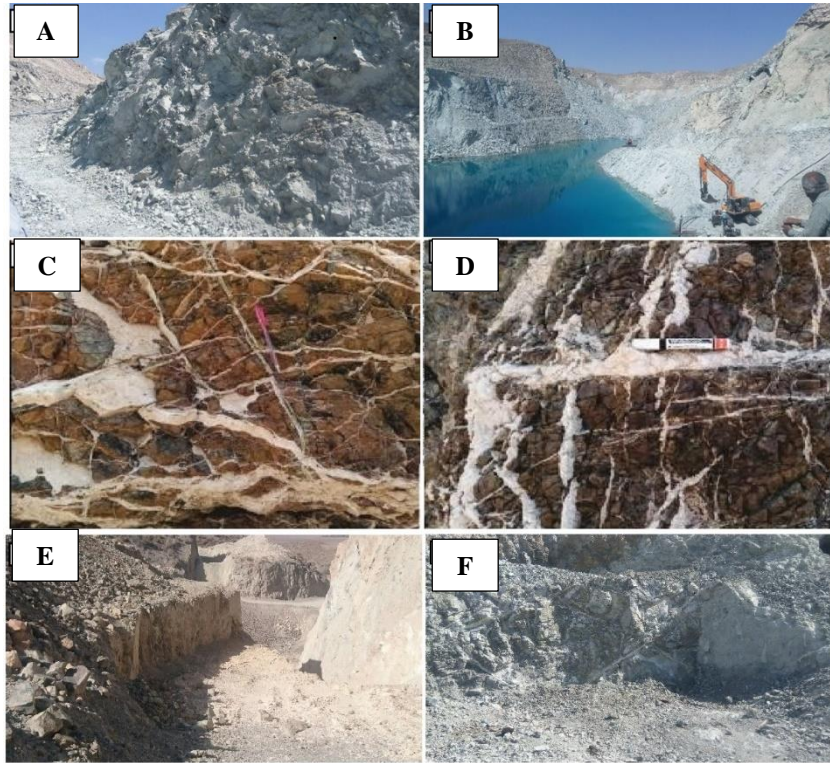
Fig. 8. A, B: The outcrop of serpentine alteration in harzburgite and dunite, north of the study area. C, D: The network of magnesite veins formed in serpentinite units. E: Outcrop of magnesite in the harzburgite. F: The outcrop of serpentine alteration in harzburgite and dunite.
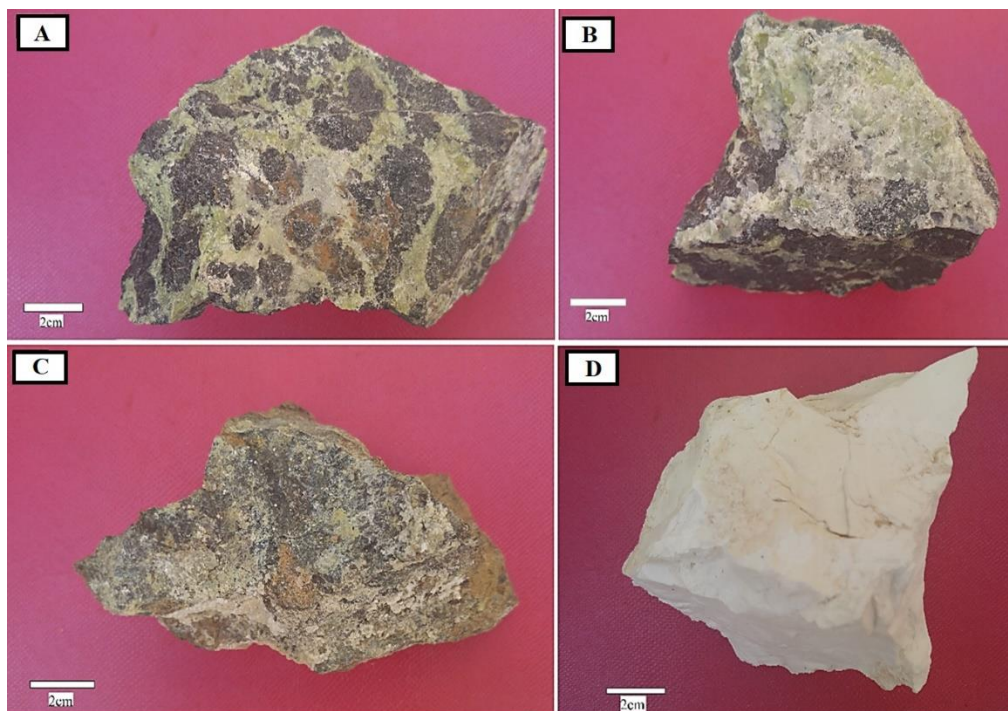
Fig. 9. A: Serpentinized specimen with chromite with leopard skin texture. B and C: Serpentinized sample of Abdasht chromite. D: A sample from magnesite veins in the northern part of the study area.

Table 3. The overall accuracy of each of the SAM and MF methods in detecting alterations

Alteration	Metude	Overall Accuracy
Serpentine	Matched Filtering (MF)	87.65%
	Spectral Angle Mapper (SAM)	81.39%
Magnesite	Matched Filtering (MF)	65.19%
	Spectral Angle Mapper (SAM)	60.63%

5. 1. Microscopic Examination Of The Collected Samples

The examination of the thin sections under microscope shows that the main minerals are olivine, serpentine and orthopyroxene. Serpentine resulting from the alteration of olivine and orthopyroxene is present in bright yellow to pale yellow in polarized light. Olivine is severely crushed due to high tectonic pressures and has many fractures. Given the presence of serpentine in association with chromite in the rock units of the area, this alteration can be used as an exploratory indicator (Figure 10).
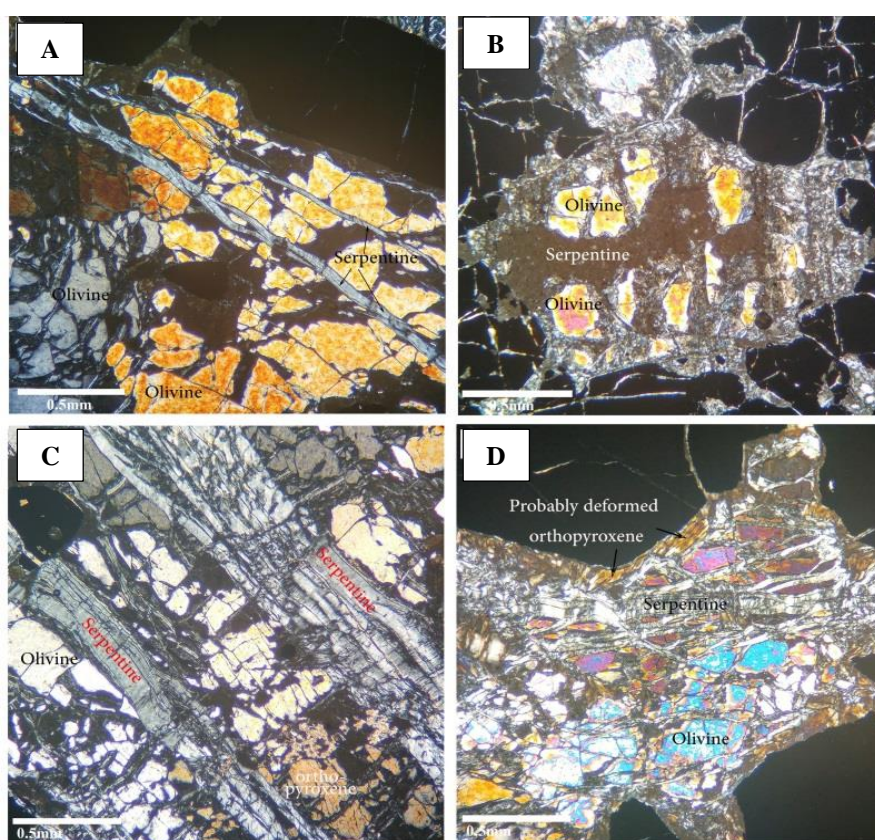
Fig. 10. Microscopic photographs of thin sections of samples taken from Abdasht chromite mine.

6. CONCLUSIONS

The results from this study indicate that hyperspectral remotely sensed images showed a good potential for chromite exploration by mapping serpentine and magnesite. The following algorithm is recommended for the pre-processing of Hyperion images: Removing the defective bands, correcting for the missing line, converting DN to radiance, smile correction, atmospheric correction by FLAASH, correcting the destripping effect, noise removal by using MNF and softening of spectra. The results in the study area showed an association of serpentine and magnesite with active chromite mines in the Abdasht area. The results obtained were confirmed by field studies, spectral examination, and thin section studies. The overall classification accuracy for MF and SAM methods was 87% and 81% for serpentine, respectively. Magnesite showed an overall accuracy of 65% and 60% for MF and SAM, respectively. Probably, the low accuracy for magnesite mineral is due to its small spatial extent. MF has more power than SAM for both serpentine alteration and magnesite detection. Due to the high resolution of Hyperion images in

exposing chromite-bearing serpentine rocks in the region, these images can be used for chromite exploration.

ACKNOWLEDGMENT

REFERENCES

[1]   Rowan, L. C., Crowley, J. K., Schmidt, R. G., Ager, C. M., & Mars, J. C. (2000). Mapping hydrothermally altered rocks by analyzing hyperspectral image (AVIRIS) data of forested areas in the Southeastern United States. Journal of Geochemical Exploration, 68(3), 145-166.

[2]   Van Der Meer, F. (2004). Analysis of spectral absorption features in hyperspectral imagery. International journal of applied earth observation and geoinformation, 5(1), 55-68.

[3]   Petrovic, A., Khan, S. D., & Thurmond, A. K. (2012). Integrated hyperspectral remote sensing, geochemical and isotopic studies for understanding hydrocarbon-induced rock alterations. Marine and Petroleum Geology, 35(1), 292-308.

[4]   Molan, Y. E., Refahi, D., & Tarashti, A. H. (2014). Mineral mapping in the Maherabad area, eastern Iran, using the HyMap remote sensing data. International Journal of Applied Earth Observation and Geoinformation, 27, 117-127.

[5]   Abdolmaleki, M., Tabaei, M., Fathianpour, N., & Gorte, B. G. (2017). Selecting optimum base wavelet for extracting spectral alteration features associated with porphyry copper mineralization using hyperspectral images. International Journal of Applied Earth Observation and Geoinformation, 58, 134-144.

[6]   Rajendran, S., Hersi, O. S., Al-Harthy, A., Al-Wardi, M., El-Ghali, M. A., & Al-Abri, A. H. (2011). Capability of advanced spaceborne thermal emission and reflection radiometer (ASTER) on discrimination of carbonates and associated rocks and mineral identification of eastern mountain region (Saih Hatat window) of Sultanate of Oman. Carbonates and Evaporites, 26(4), 351-364.

[7]   Tangestani, M. H., Jaffari, L., Vincent, R. K., & Sridhar, B. M. (2011). Spectral characterization and ASTER-based lithological mapping of an ophiolite complex: A case study from Neyriz ophiolite, SW Iran. Remote Sensing of Environment, 115(9), 2243-2254.

[8]   Hashim, M., Pournamdary, M. and Pour, A. B. (2011) Processing and interpretation of advanced space-borne thermal emission and reflection radiometer (ASTER) data for lithological mapping in ophiolite complex. Int. J. Phys. Sci., 6, 6410– 6421 .

[9]   Rajendran, S., Al-Khirbash, S., Pracejus, B., Nasir, S., Al-Abri, A. H., Kusky, T. M., & Ghulam, A. (2012). ASTER detection of chromite bearing mineralized zones in Semail Ophiolite Massifs of the northern Oman Mountains: Exploration strategy. Ore geology reviews, 44, 121-135.

[10]   Rajendran, S., Nasir, S., Kusky, T. M., Ghulam, A., Gabr, S., & El-Ghali, M. A. (2013). Detection of hydrothermal mineralized zones associated with listwaenites in Central Oman using ASTER data. Ore geology reviews, 53, 470-488

[11]   Pournamdari, M., Hashim, M., & Pour, A. B. (2014). Spectral transformation of ASTER and Landsat TM bands for lithological mapping of Soghan ophiolite complex, south Iran. Advances in Space Research, 54(4), 694-709.

[12]   Barry, P. (2001) EO-1/Hyperion Science Data User's Guide. TRW Space, Defense & Information Systems, Redondo Beach, CA.

[13]   Kruse, F. A., Boardman, J. W., & Huntington, J. F. (2003). Comparison of airborne hyperspectral data and EO-1 Hyperion for mineral mapping. IEEE transactions on Geoscience and Remote Sensing, 41(6), 1388-1400.

[14]   Stocklin, J. 1968- Structural history and tectonics of Iran . A review; Amer. Assoc. Petrol. Geol. Bull., P. 1229-1258

[15]   Paragon Co. 1974- Explanatory text of Minab quadrangle map 1: 250000 : Geol. Surv. Iran.

[16]   Najafzadeh, Ali and Hamid Ahmadipour. "Using platinum-group elements and Au geochemistry to constrain the genesis of podiform chromitites and associated peridotites from the Soghan mafic–ultramafic complex, Kerman, Southeastern Iran." Ore Geology Reviews 60 (2014): 60-75.

[17]   Barry, P. S., Mendenhall, J., Jarecke, P., Folkman, M., Pearlman, J., & Markham, B. (2002, June). EO-1 Hyperion hyperspectral aggregation and comparison with EO-1 Advanced Land Imager and Landsat 7 ETM+. In IEEE International Geoscience and Remote Sensing Symposium (Vol. 3, pp. 1648-1651). IEEE.

[18]   Ducart, D. F., Silva, A. M., Toledo, C. L. B., & Assis, L. M. D. (2016). Mapping iron oxides with Landsat-8/OLI and EO-1/Hyperion imagery from the Serra Norte iron deposits in the Carajás Mineral Province, Brazil. Brazilian Journal of Geology, 46(3), 331-349.

[19]   Goodenough, D. G., Dyk, A., Niemann, K. O., Pearlman, J. S., Chen, H., Han, T., ... & West, C. (2003). Processing Hyperion and ALI for forest classification. IEEE transactions on geoscience and remote sensing, 41(6), 1321-1331.

[20]   Ghaffari, O., Vadan Zoj, M. J., Mokhtarzadeh, M., (2016), Radiometric Corrections of Hyperion High-Definition Images in order to extract information on geological applications. Second National Conference on Spatial Information Technology Engineering, Tehran, Faculty of Mapping Engineering, Khajeh Nasir al-Din Tusi University of Technology (in Persian)

[21]   Liang, S. & Li, X. & Wang, J. (2012). Advanced Remote Sensing. 10.1016/C2010-0-67304-4.

[22]   Kruse FA, Lefkoff AB, Boardman JB, Heidebrecht KB, Shapiro AT, Barloon PJ, Goetz A.F.H (1993)The Spectral Image Processing System (SIPS) – interactive visualization and analysis of imagingspectrometer data, Remote Sensing of Environment 44: 145–163.

[23]   Tangestani MH, Mazhari N, Agar B, Moore F (2008) Evaluating Advanced Spaceborne Thermal Emission and Reflection Radiometer (ASTER) data for alteration zone enhancement in a semi-arid area, northern Shahr–e–Babak, SE Iran, International Journal of Remote Sensing 29: 2833–2850.

[24]   Saed, S., Azizi, H., Daneshvar, N., Afzal, P., Whattam, S.A., Mohammad, Y.O., 2022 Hydrothermal alteration mapping using ASTER data, Takab-Baneh area, NW Iran: A key for further exploration of polymetal deposits. Geocarto International, 1-25 doi/abs/10.1080/10106049.2022.2059110.

[25]   Mirsepahvand, F., Jafari, M.R., Afzal, P., Arian, M.A., 2022. Identification of Alteration Zones using ASTER Data for Metallic Mineralization in Ahar region, NW Iran. Journal of Mining and Environment 13(1), 309-324
http://dx.doi.org/10.22044/jme.2022.11477.2135

[26]   Fakhari, S., Jafarirad, A., Afzal, P., & Lotfi, M. (2019). Delineation of hydrothermal alteration zones for porphyry systems utilizing ASTER data in Jebal-Barez area, SE Iran. Iranian Journal of Earth Sciences, 11(1), 80-92.

[27]   Boardman, J. W., 1993, Automated spectral unmixing of AVIRIS data using convex geometry concepts: in Summaries, Fourth JPL Airborne Geoscience Workshop, JPL Publication 93-26, v. 1, p. 11-14

[28]   Huntington, J. F. and Boardman, J. W., (1995), Semi-quantitative Mineralogical and geological mapping with 1995 AVIRIS data, Proc. Spectral Sensing Research '95, ISSSR, Published by the AGPS, 26 Nov - 1 Dec, 1995, Melbourne, Australia.

[29]   Boardman, J. W., (1997), Mineralogic and geochemical mapping at Virginia City, Nevada using 1995 AVIRIS data, in Proceedings of the Twelfth Thematic Conference on Geological Remote Sensing, Environmental Research Institute of Michigan, Denver, CO, pp. 21-28.

[30]   Kruse, F. A., Boardman, J. W., & Huntington, J. F. (2003). Comparison of airborne hyperspectral data and EO-1 Hyperion for mineral mapping. IEEE transactions on Geoscience and Remote Sensing, 41(6), 1388-1400.

[31]   Harsanyi, J. C., Chang, C. I., 1994, Hyperspectral image classification and dimensionality reduction: an orthogonal subspace projection approach. IEEE Transactions on Geoscience and Remote Sensing, Vol. 32, pp. 779–785.

[32]   Ferreir, G., White, K., Griffiths, G., Bryant, r., Stefofuli, M., 2002, The mapping of hydrothermal alteration zones on the island of Levos, Greece using an integrated remote sensing dataset, International of journal of Remote sensing, Vol. 23, pp. 341-356.

[33]   Adeli, Z., Rassa, I., Darvishzadeh, A., 2008, Application of matched filtering technique to target alteration minerals. 29th Asian Conference on Remote Sensing (ACRS), Srilanka..

[34]   Darhkordi, M, 1400. "Evaluation of structural control in the placement of chromite deposits in the southern part of Abdasht ultramafic massif (south of Baft city)". Master's thesis, Kerman University, 53 pages.